DOI 10.1007/s11141-017-9740-z
Radiophysics and Quantum Electronics, Vol. 59, No. 8–9, January–February, 2017
(Russian Original Vol. 59, No. 8–9, August–September, 2016)

THE FEATURES OF THE FREQUENCY-MODULATION METHOD WHEN STUDYING THE SHAPES OF THE SPECTRAL LINES OF NONLINEAR ABSORPTION

G. Yu. Golubiatnikov,* S. P. Belov, and A. V. Lapinov

UDC 535.14

We briefly consider the method of the frequency (phase) modulation and signal detection at the second harmonic of the modulation frequency for recording and analyzing the spectral-line shapes. The precision sub-Doppler spectrometer in the millimeter- and submillimeter-wave ranges, which operated in the regime of nonlinear saturation of the spectral transitions in a standing wave (the Lamb-dip method), was used during the measurements. The influence of the saturation degree on the value and shape of the recorded frequency-modulated signals in the quadrature channels during the synchronous detection is demonstrated. Variation in the relationships among the signals determined by dispersion and absorption was observed. The necessity of allowance for the influence of the group-velocity dispersion and coherent effects on the shape of the recorded spectral lines is experimentally shown.

1. INTRODUCTION

The methods of nonlinear absorption of radiated power, which allow one to substantially improve the Doppler-broadening-limited resolution, are used for obtaining the precision laboratory values of the frequencies of the molecular transitions and studying their hyperfine structure. The Lamb-dip method (see [1] and the references therein) allows one to obtain a narrow nonlinear resonance exactly at the spectral-line center as a result of the saturation populations of the molecule-transition levels by the counterpropagating waves. In this case, the measurement accuracy of the center frequencies of the molecular transitions is considerably improved [2], and it becomes possible to study the hyperfine structure inside the Doppler line, which is of interest for the ground-based and space radio astronomy [3].

The Lamb-dip contrast (i.e., the ratio of the amplitude decrease at the line center to the general amplitude) in the contour of the line, which is broadened as a result of the Doppler effect, does not usually exceed 13% [4]. To increase the contrast and, therefore, the signal-to-noise ratio, the frequency modulation of the radiation transmitted through the gas is used [5, 6]. A sinusoidal variation in the radiation frequency $\nu(t) = \nu + \Delta \sin(2\pi\nu_{\rm m}t)$, where ν is the radiation frequency, $\nu_{\rm m}$ is the modulation frequency, $\Delta = \delta\,\nu_{\rm m}$ is the frequency deviation, and δ is the modulation index, is usually used. The frequency-modulation method is also widely used in conventional linear direct-absorption spectroscopy in order to increase the signal-to-noise ratio, improve the frequency resolution, and decrease the base-line influence. In addition, the frequency-modulation method is very sensitive to variations in the line shape compared with, e.g., amplitude modulation since the line-related signal at the second harmonic $2\nu_{\rm m}$ of the modulation frequency is proportional to the second derivative of the line contour.

* glb@appl.sci-nnov.ru

Institute of Applied Physics of the Russian Academy of Sciences, Nizhny Novgorod, Russia. Translated from Izvestiya Vysshikh Uchebnykh Zavedenii, Radiofizika, Vol. 59, No. 8–9, pp. 798–810, August–September 2016. Original article submitted April 26, 2016; accepted July 25, 2016.

0033-8443/17/5908-0715 © 2017 Springer Science+Business Media New York

The quantitative information is extracted from the experimental records of the spectral-line contours by analyzing the theoretical model of the contour. In the simplest case, the nonlinear resonance for low gas pressures can be described as an absorption decrease at the center of the Doppler-broadened line. This decrease has the Lorentz-contour shape with the width determined by the molecular collisions. The results given in [7–9] are indicative of the considerable difference between the collisional coefficients of the nonlinear-resonance broadening at small pressures in CO_2 and CH_4 compared with the linear-absorption line at high pressures. This discrepancy of the broadening coefficients is attributed to a contribution of the particles with small-angle scattering to the collision integral and diffraction scattering [9]. This makes the Lamb-dip method attractive for studying the influence of the different-type molecular collisions on the nonlinear-resonance shape compared with the linear case where the line-shape variations amount to only several percent [10].

On the other hand, for low pressures, the time of the particle interaction with the field can be determined by the transit time $\tau = a/V_0$ rather than collisions, where a is the beam radius, $V_0 = \sqrt{2k_{\rm B}T_0/M_{\rm m}}$ is the velocity of a molecule with the mass $M_{\rm m}$, $k_{\rm B}$ is Boltzmann's constant, and T_0 is the gas temperature in a cell. For $\Gamma\tau \ll 1$ (Γ is the collision-determined homogeneous line half-width) and a small saturation parameter $G < 1$ (i.e., the ratio of the radiated power to the saturation power), the nonlinear-resonance width is determined by the expression $\gamma = 1.51(\Gamma/\tau)^{0.5}$ differing from the expression $\gamma = \Gamma(1+G)^{0.5}$ [11–13], which is valid for $\Gamma\tau > 1$. Under the above-mentioned conditions, only very slow particles with the effective temperature $T_{\rm eff} = (\Gamma\tau)^2 T_0$ interact with the radiation field, which allows one to obtain very narrow resonances (with the linewidth below 100 Hz) [14, 15]. However, since the resonance intensity considerably drops at low pressures (proportionally to p^3 [12]), it is rather difficult to realize this regime using a conventional spectrometer.

If the nonlinear-resonance width is comparable with the inverse time of the frequency tuning over the line (Δ or $\nu_{\rm m} \gg \gamma$), one should allow for not only the modulation distortions of the spectrum of the frequency-modulated signal, but also the influence of the nonstationary effects, such as the time beats of the frequency components. Therefore, if the time of the population oscillations between the levels numbered n and m, which is determined by the Rabi frequency $g = d_{nm}E/\hbar$, is shorter than the relaxation time ($g > \Gamma$), the coherent transition effects, such as stimulated emission of the molecules should be taken into account (here, d_{nm} is the dipole moment of the spectral transition, E is the intensity of the radiated electric field, and $\hbar$ is Planck's constant). In the nonlinear case, this phenomenon for the pulsed radiation is known as a self-induced transparence effect for the 2π pulses [16, 17], in which a considerable slowing down of the perturbation-pulse propagation through the absorbing medium is observed.

It should be noted that the above-mentioned effects in the millimeter- and submillimeter-wave ranges can be observed simultaneously since the Lamb-dip method is restricted by the low pressures $p \leq$ 1–3 mTorr because of the relatively small Doppler broadening (0.1–1.0 MHz) compared with the homogeneous collisional broadening (the typical broadening coefficient is 3–20 kHz/mTorr). If the radiation-source intensity is about 1 mW/cm^2, the Rabi frequency amounts to about 30 kHz even for the weak transitions (the dipole moment for a CO molecule is $d \approx 0.1$ D), which imposes certain restrictions on the radiated power and the frequency-modulation parameters when studying various physical processes.

In the literature, the frequency-modulation spectroscopy is divided into two types according to the modulation method of the laser radiation. The ratio of the modulation frequency to the width of the studied spectral line ($2\,\Delta\nu$) is the division criterion [18]. The frequency modulation corresponds to the case where the modulation frequency is much greater than the linewidth [19, 20]. In this case, the modulation index is usually chosen as $\delta < 1$, i.e., only two side frequencies are present in the radiation spectrum. This modulation method is used for reaching maximum sensitivity (the modulation frequency exceeds the range of the low-frequency noise including the shot noise) when the absorbing cell is compatible with the high-quality resonator [21, 22] and the side-frequency spectrum coincides with the frequency interval of the resonator modes.

The wavelength modulation corresponds to the case where the modulation frequency does not exceed

the linewidth [23, 24]. In this case, the frequency deviation is most frequently chosen close to the linewidth when the line-related signal is maximum and the line-shape distortions are not too large because of the modulation broadening. If the modulation frequency is much lower than the linewidth, the modulation-frequency influence on the line shape can be neglected. This is the case of the so-called "frozen" modulation [5, 25]. For the unsaturated Lorentz line ($\nu_{\rm m} \ll \Delta\nu_{\rm L}$), there exist analytical contour models for both the first two modulation harmonics [26, 27] and the higher harmonics ($n\nu_{\rm m}$, where $n > 2$) [5, 23] in the case of an arbitrary frequency deviation. For the Doppler contour, the analytical expressions become more complicated [24, 29], whereas the numerical calculations [29] or the approximate expressions [31] are usually used for the Voigt profile.

If the modulation frequency is comparable with the linewidth ($\nu_{\rm m} \sim \Delta\nu$), in the case of synchronous detection, the demodulated frequency-modulated signal related to the line is determined by not only absorption but also dispersion, while the resulting profile of the line also depends on the phase difference of the modulation and reference-signal frequencies.

Under the condition of optical saturation of the spectral transitions, the standard Doppler, Lorentz, and Voigt profiles vary under the action of incident radiation. As was mentioned above, for a small saturation parameter $G < 1$, the Lamb contour can be represented with good approximation as a sum of the Doppler and Lorentz contours. For a large saturation parameter ($G > 1$), the analysis and choice of an adequate model describing the line contour become more complicated. It is shown in [32–34] that for the saturation line, the relationship between the dispersion and absorption is no longer described by the Kramers–Kronig relations. An increase in the contrast of the dispersion part (or phase) of the Lamb dip up to 0.45 is observed for $G \gg 1$ compared with the maximum contrast for the absorption coefficient, which is equal to 0.13, for $G = 1.4$.

Despite the complexity and ambiguity of the line-shape analysis at low pressures ($\Gamma\tau \ll 1$) and $G > 1$, the frequency-modulation method has no rivals when studying the physical processes of the radiation–matter interaction.

In what follows, we show the examples of the measurements of the spectral lines, which demonstrate the nonlinear-absorption influence on their shape and the signal phase in the quadrature channels during the synchronous detection. The possible influence of the coherent effects and the dispersion of the group velocity of the radiation on the line profiles is considered. Since a significant decrease in the group velocity of the radiation is observed in the narrow spectral lines (see, e.g., the experiments with slow light [35]), in this work we present estimates of the group-velocity variation for the CO-molecule transition $J = 3 \leftarrow 2$.

2. SHAPE OF THE SIGNAL RELATED TO THE SPECTRAL LINE DURING FREQUENCY MODULATION

The spectrum of the field of the frequency-modulated radiation can be represented as a series in terms of the modulation-frequency harmonics $\nu \pm n\nu_{\rm m}$:

$$E(t) = E_0 \exp\{i[\omega t + \delta \sin(2\pi\nu_{\rm m} t)]\} = E_0 \sum_{n=-\infty}^{\infty} J_n(\delta) \exp[i(\omega + n2\pi\nu_{\rm m})t], \tag{1}$$

where $\omega = 2\pi\nu$ is the angular frequency of the radiation and J_n is a Bessel function. The even ($\nu \pm 2n\nu_{\rm m}$, $\nu \pm 4n\nu_{\rm m}$, ...) and odd ($\nu \pm n\nu_{\rm m}$, $\nu \pm 3n\nu_{\rm m}$, ...) harmonics of the side frequencies are in quadrature (the phase difference is $\pi/2$). The signal demodulation and the line recording are performed with the help of a lock-in amplifier. This amplifier is a phase detector such that the radiation signal from the photoreceiver and the reference signal at the modulation frequency are supplied to its one and the other inputs, respectively. The output signal is proportional to the quantity $I(\omega)\cos(\Delta\phi)$, where $I(\omega)$ is the signal transmitted through the sample and $\Delta\phi$ is the phase difference between the modulating and reference signals. The absorption line itself serves as the frequency discriminator. To exclude information loss, the following quadrature technique is used: two phase detectors whose reference-signal phases are shifted with respect to each other by $\pi/2$ are

used, whereas the recorded signals are proportional to $I(\omega)\cos(\Delta\phi)$ and $I(\omega)\sin(\Delta\phi)$.

The measurements were performed using the wavelength modulation method, i.e., the line did not split into individual spectral components ($\nu_{\rm m}/\Delta\nu < 1$). In the approximation of low modulation frequency ("frozen" modulation) if the distance between the side frequencies is smaller than the linewidth, i.e., $\nu_{\rm m}/\Delta\nu \ll 1$, the Lorentz contour at the second modulation harmonic in the linear case can be written in the form [5]

$$K_2(\Omega) = \frac{S}{\pi}\mathrm{Re}\left\{[\Delta^2 + (\Delta\nu_{\rm L} + i\Omega)^2]^{-1/2} \right. \\ \left. -2\Big/\left[\Delta\nu_{\rm L} + i\Omega + \sqrt{\Delta^2 + (\Delta\nu_{\rm L} + i\Omega)^2} + \Delta^2/(\Delta\nu_{\rm L} + i\Omega)\right]\right\}^{-1}. \quad (2)$$

Here, S is the amplitude ν_0 at the line center, $\Omega = \nu - \nu_0$ is the frequency detuning from the line center, and the line half width $\Delta\nu_{\rm L} = \Gamma$. This expression holds for an arbitrary frequency deviation and can be used with good approximation for the modulation frequencies $\nu_{\rm m}/\Delta\nu_{\rm L} < 0.2$. The dependence of the amplitude of the signal at the second harmonic on the frequency deviation Δ is nonmonotonic [27, 28]. With increasing deviation, the signal increases and reaches its maximum for $\Delta/\Delta\nu_{\rm L} \approx 2.2$. In this case, the recorded-line half-width $\Delta\nu \approx \Delta\nu_{\rm L}$. Then the amplitude slowly decreases with increasing deviation, and the linewidth continues to increase. Although the equations given in [27–29] somewhat differ from Eq. (2) in form, they all yield identical results.

Although the modulation frequency does not enter Eq. (2), the frequency-modulation signals are determined by both the absorption coefficient S_l and the refractive index (dispersion) D_l of the medium for an arbitrary ratio $\nu_{\rm m}/\Delta\nu$. The quadrature-channel signals $I_{\cos_l}(\Omega,\varphi)$ and $I_{\sin_l}(\Omega,\varphi)$, which are called the cosine and sine signals, respectively, are written as

$$I_{\cos_l}(\Omega,\varphi) = -S_l(\Omega)\cos\varphi + D_l(\Omega)\sin\varphi, \qquad I_{\sin_l}(\Omega,\varphi) = S_l(\Omega)\sin\varphi + D_l(\Omega)\cos\varphi, \quad (3)$$

where $\varphi = \Delta\phi + \Phi$ is the phase difference between the reference modulation signal and the detector signal, Φ is the random phase, and l is the modulation-frequency harmonic number. For the Lorentz contour, the expressions for S_l and D_l can be represented as the series (see [5])

$$S_l(\Omega) \propto -\sum_{n=-M+1}^{M-1} J_n(\delta)J_{n-l}(\delta)(\alpha_n + \alpha_{n-l}), \qquad D_l(\Omega) \propto \sum_{n=-M+1}^{M-1} J_n(\delta)J_{n-l}(\delta)(\beta_{n-l} - \beta_n). \quad (4)$$

The coefficients α_n and β_n are determined by the formulas

$$\alpha_n = \frac{1}{1 + (\Omega + n\nu_{\rm m})^2/\Delta\nu_{\rm L}^2}, \qquad \beta_n = \frac{(\Omega + n\nu_{\rm m})/\Delta\nu_{\rm L}}{1 + (\Omega + n\nu_{\rm m})^2/\Delta\nu_{\rm L}^2}. \quad (5)$$

Equation (4) ensures an approximation accuracy of about 10^{-4} for $M = [1.8\delta + 3.4]$, where the square brackets denote the integer part. The number of the expansion terms is proportional to the modulation index $M \propto \delta$.

The signal related to the spectral line can also be recorded in the form of the amplitude $I(\Omega) = \sqrt{[I_{\cos}(\Omega,\varphi)]^2 + [I_{\sin}(\Omega,\varphi)]^2}$ and the argument $\psi(\Omega,\varphi) = \arctan[I_{\sin}(\Omega,\varphi)/I_{\cos}(\Omega,\varphi)]$. In what follows, the quantity $\psi(\Omega,\varphi)$ is called the phase line. The form of the function $\psi(\Omega)$ is independent of the modulation phase φ. The phase line also contains information on the relationship between the absorption signal $S_l(\Omega)$ and the dispersion signal $D_l(\Omega)$.

The characteristic profiles of the Lorentz line at the second modulation harmonic for $I_{\sin_2}(\Omega,0)$, $I_{\cos_2}(\Omega,0)$, $I(\Omega)$, and $\psi(\Omega)$. For the modulation frequencies that are small compared with the linewidth, the dependence $\psi(\Omega)$ (Fig. 1*c*) has the Π-shaped profile, and the phase difference between the line wings and the center (i.e., the line swing) is approximately equal to π. The slopes of the line of $\psi(\Omega)$ become smoother

with increasing modulation frequency and radiated power, as it is obvious for the Doppler contours in the corresponding panels of Figs. 2 and 3, while the phase-line swing increases (becomes greater than π).

Note that for $\nu_{\rm m}/\Delta\nu_{\rm L} < 0.01$ the ratio of the maximum dispersion and absorption signals at the second modulation harmonic is written as $D_2(0)/S_2(0) < 0.03$, i.e., the dispersion-term influence can be neglected. However, for $\nu_{\rm m}/\Delta\nu_{\rm L} = 0.1$, this ratio is no longer small ($D_2(0)/S_2(0) = 0.3$). Therefore, in order to use analytical expression (2), the modulation phase φ should be tuned in such a way that only the absorption signal $S_2(\Omega)$ is present in one channel and only the signal $D_2(\Omega)$ is present in the other channel (see Eq. (3)). In the case of an arbitrary ratio $\nu_{\rm m}/\Delta\nu_{\rm L}$, Eqs. (3)–(5) should be used instead of Eq. (2).

The above analysis for the Lorentz contour is also qualitatively valid for other line profiles (the Doppler and Voigt contours) with the Lamb dip, but the formulas become more awkward. For the Lamb dip, the expression for line shape is given by Eq. (20) in [5] as a function of the saturation coefficient. It is seen in Figs. 3 and 4 of [5] that in the case where the Lamb-dip width differs only slightly from the Doppler-contour width (about $0.1\,\Delta\nu$), the Lorentz-contour distortion is observed already for the relatively small saturation parameter $G \approx 0.2$ since the Lamb-dip depth increases and the Doppler-line amplitude deceases with increasing G. For a large Doppler broadening ($\Delta\nu_{\rm D} \gg \gamma$), the Lamb dip can be considered as a Lorentz line on the parabolic profile.

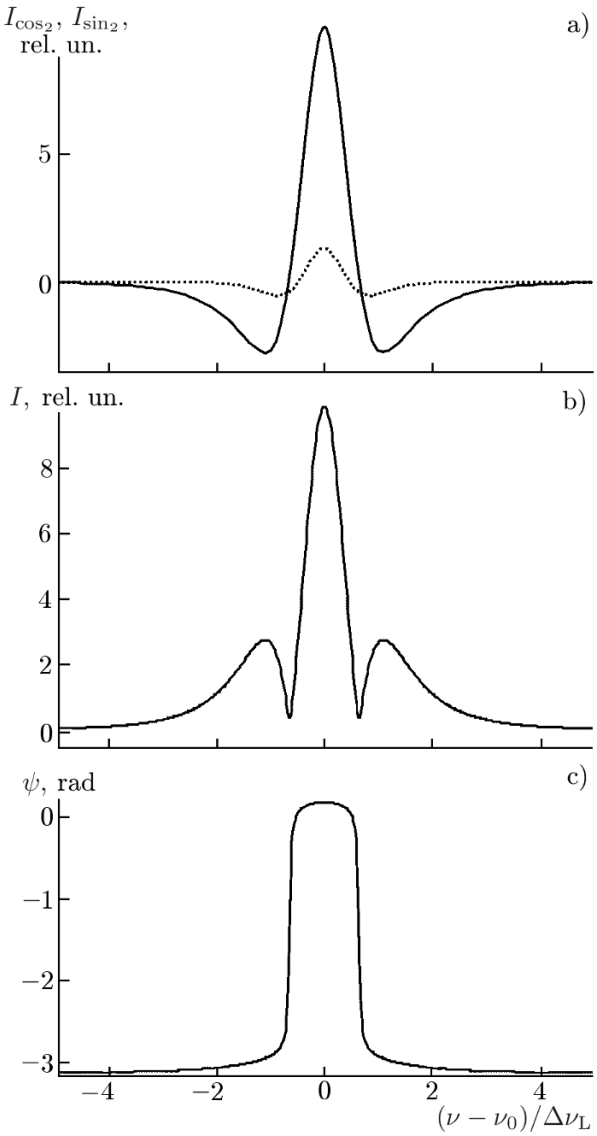

Fig. 1. Calculated profiles of the Lorentz line at the second harmonic of the modulation frequency for $\nu_{\rm m}/\Gamma = 0.05$ and $\delta = 10$: the amplitude $I_{\cos_2}(\Omega, \varphi = 0)$ and the dispersion $I_{\sin_2}(\Omega, \varphi = 0)$ (the solid and dotted lines, respectively) (*a*) and the absolute values of the signal amplitude (*b*) and the phase $\psi(\Omega)$ (*c*).

3. EXPERIMENTAL RESULTS

In this work, we use a sub-Doppler direct-absorption microwave spectrometer [1]. As the radiation is transmitted through an absorbing gas layer with thickness L (the cell length and diameter in the experiment are $L_0 = 200$ cm and 11 cm, respectively), the radiation intensity decreases according to the exponential law (the Bouguer–Lambert–Beer law) $I(\Omega) = I_0(\Omega)\exp[-\alpha(\Omega)L]$, where $I_0(\Omega)$ is the incident-radiation intensity and $\alpha(\Omega)$ is the absorption index in the spectral line. The backward-wave oscillator (BWO) was used as the radiation source. The absolute accuracy and stability of the BWO frequency is determined by the parameters of the reference-standard signal with a frequency of 10 MHz. In our case, the long-term stability of the rubidium standard was about $3\cdot10^{-12}$, while the spectral width of the BWO radiation was less than 10 Hz, which allowed us to measure narrow spectral lines.

The frequency-modulated radiation, which is transmitted through the sample, is reflected by the angle reflector, forms the standing wave in a cell, and is directed to a quadrature detector or cooled bolometer (the temperature is 4.2 K), using the wire polarizer. A lock-in amplifier with quadrature reception was used for the signal demodulation and the two-channel recording of the line was performed at the second modulation

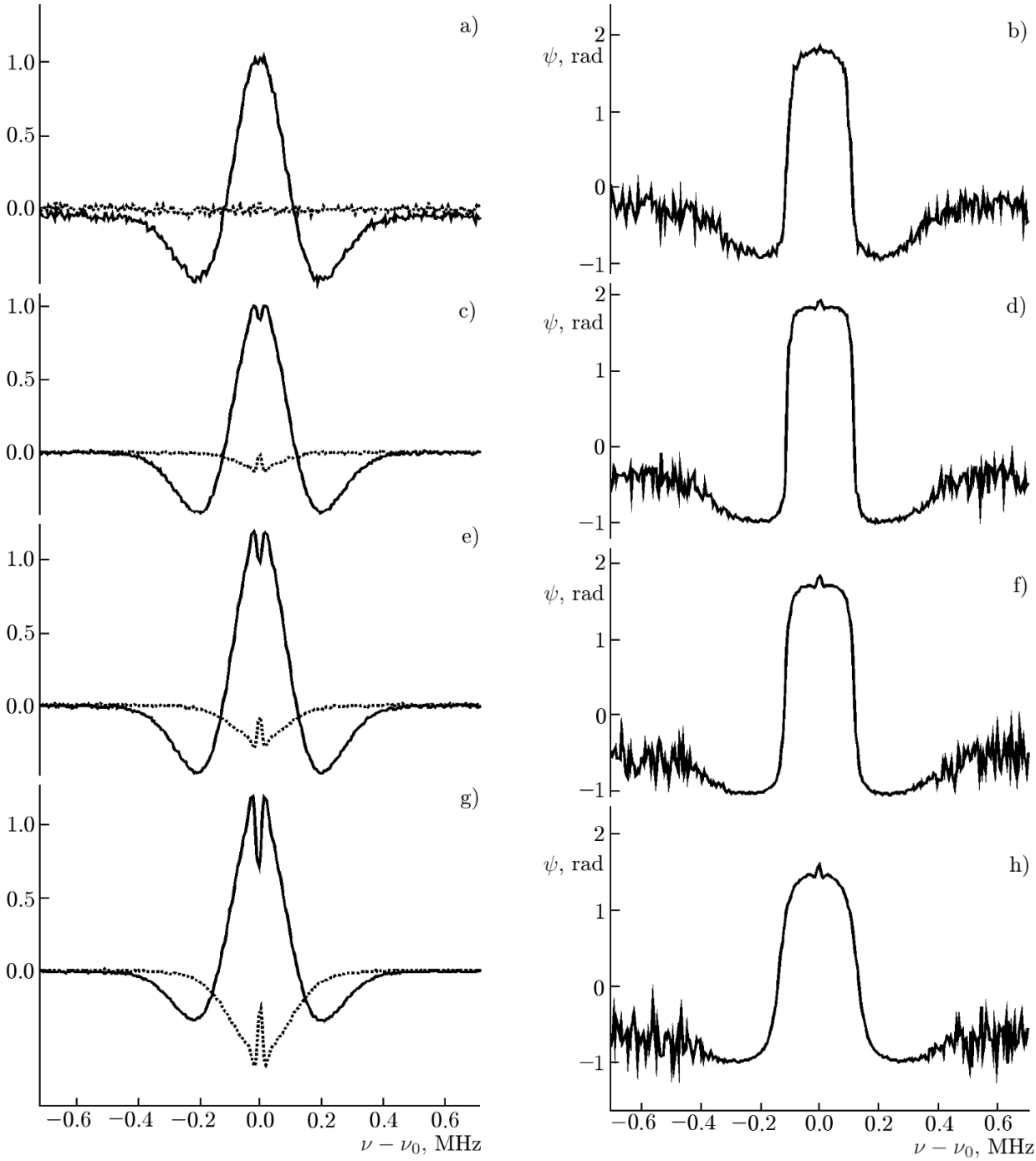

Fig. 2. Frequency dependences of the amplitude (*a*, *c*, *e*, and *g*; the solid lines correspond to the channel $I_{\cos_2}$ and the dotted lines, to $I_{\sin_2}$) and the phases ψ (*b*, *d*, *f*, and *h*) of the signal related to the CO-molecule line at a frequency of 115 GHz ($J = 0 \leftarrow 1$) for the radiated powers $P = P_0$ (*a* and *b*), P_1 (*c* and *d*), P_2 (*e* and *f*), and P_3 (*g* and *h*), $P_3 > P_2 > P_1 > P_0$, $\nu_m = 3.3$ kHz, $p \approx 2.5$ mTorr, and $\Delta = 15$ kHz. The line amplitudes are normalized to unity and the phase-line variation interval remained almost unchanged for this power range and amounted to about 2.5 rad.

harmonic of the radiation frequency.

A simple model of the second derivative of the Lamb-dip contour in the Doppler line can be used in the case of a small frequency deviation ($\Delta/\Delta\nu \ll 1$ and $\nu_m/\Delta\nu \ll 1$) and a small saturation ($G < 1$) to adjust the lines to the model profile. However, deviation from the model profile was observed already at

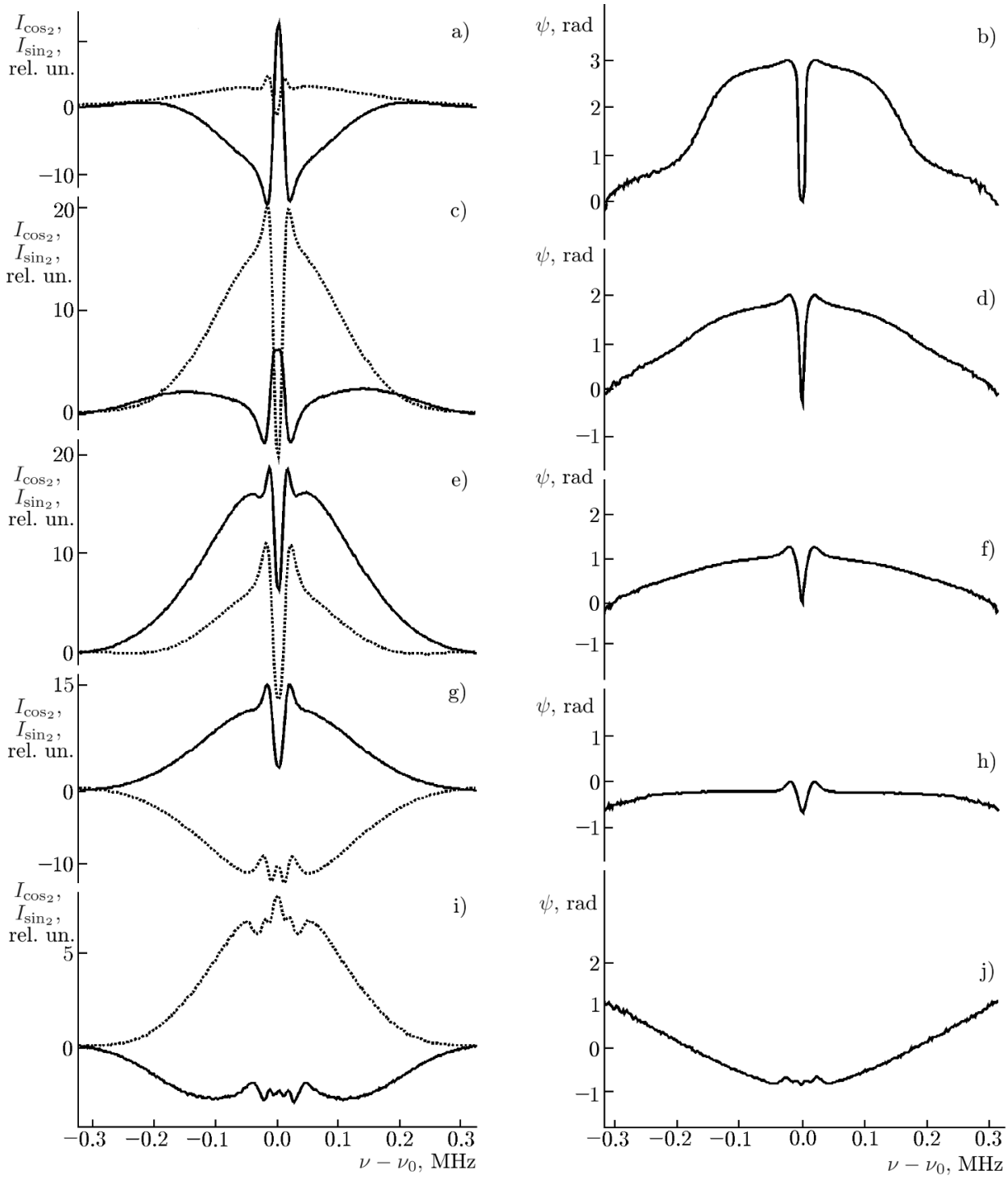

Fig. 3. Records of the amplitude (*a*, *c*, *e*, *g*, and *i*; the solid lines correspond to the channel $I_{\cos_2}$ and the dotted lines, to $I_{\sin_2}$) and the phases ψ (*b*, *d*, *f*, *h*, and *j*) of the signal related to the OCS-molecule line at a frequency of 145 GHz ($J = 12 \leftarrow 11$) for various modulation frequencies: $\nu_{\rm m} = 2.5$ kHz (*a* and *b*), 5 kHz (*c* and *d*), 7.5 kHz (*e* and *f*), 10 kHz (*g* and *h*), 20 kHz (*i* and *j*). The pressure $p \approx 1$ mTorr and $\Delta = 10$ kHz.

$G \sim 1$ not only for the Lamb lines, but also the Doppler contour. In this case, the line shape, which was recorded in the form of the line of the phase $\psi(\Omega)$, was subject to a stronger variation.

When measuring the lines for $G \geq 1$, the following effects, which are not explained by the above-described model of the line profile at the second harmonic of the modulation frequency, are observed.

1. The demodulation phases of the Doppler contour and the Lamb dip do not coincide and the difference between these phases is a function of the pressure and power.

2. The frequency behavior of variation in the line of the phase $\psi(\Omega)$ differs from the theoretical one, i.e., an additional signal-phase increment in the central part of the line is observed and the signal delay is a function of the modulation frequency.

3. For low pressures, the Doppler-contour shape has the Gaussian form rather than the shape of the second derivative of that profile. For low pressures (in the transit-effect region), the Lamb-dip line is no longer of Lorentz type and becomes similar to the shape of the contour itself rather than its second derivative.

4. For the modulation frequencies comparable with or exceeding the saturation-line width, the Doppler-contour beats with the power-dependent amplitude are observed in the neighborhood of the Lamb dip.

Figure 2 shows the nonlinear dependence for the contrast of the Lamb dip of the Doppler contour for the amplitudes and the lines of the phases $\psi(\Omega)$. For the linear case, the phase is chosen such (Fig. 2*a*) that the sine signal (dotted line) is equal to zero, i.e., $I_{\sin_2}(\Omega, \varphi) = 0$. Variation in the modulation phase, which is manifested as an increase in the signal in the sine channel, is observed with increasing power. Variation in the Lamb-line phase is more pronounced than that of the Doppler line. With increasing power, the line shape of the phases $\psi(\Omega)$ for the Doppler contour becomes smoother and the Lamb line on the Doppler contour is observed as an increase in the signal rather than its decrease.

Figure 3 presents a series of the dependences of the amplitudes and the phases $\psi(\Omega)$ on the modulation frequency. Sign reversal of the line phase $\psi(\Omega)$ is observed with increasing modulation frequency. In this case, the signal related to the Lamb line is observed as a dip rather than signal increase in the line (see Fig. 2). Therefore, the modulation phase can be chosen so that an increase in the signal amplitude on the Doppler contour occurs instead of the dip (see, e.g., the dotted line in Fig. 3*i*). The Lamb-line splitting (Figs. 3*g*–3*j*) agrees with the considered theoretical model (Eqs. (3)–(5); also see Fig. 7 in [5]). The frequency dependence of the absorption line for the Doppler line has a shape that is close to the Gaussian one (instead of its second derivative), which can be related to the Doppler-line distortion because of the collision-frequency dependence on the particle velocity and the different influence of the transit effect on the line center and wings.

The observed dependences $I_{\cos_2}(\Omega, \varphi)$, $I_{\sin_2}(\Omega, \varphi)$, and $\psi(\Omega)$ are often difficult to explain within the framework of the theoretical model used in this work. For example, variation in the line shape of the phase $\psi(\Omega)$ under various experimental conditions can be attributed to the fact that the relationship between the absorption and dispersion, which are related by the Kramers–Kronig relations in the linear case, is changed in the nonlinear regime. It can also be explained by variation in the phase φ along the line contour, i.e., the frequency dependence of the modulation phase $\varphi(\Omega)$, which in turn can be due to variation in the group velocity of the radiation at the spectral-transition frequency.

Therefore, there exists ambiguity in interpreting the causes of variation in the amplitudes and forms $I_{\cos_2}(\Omega, \varphi)$ and $I_{\sin_2}(\Omega, \varphi)$ due to the Lamb dip of the signals on the Doppler contour. The observed dependences are related to variations in either the relative linewidths and the saturation degree, which are determined by the pressure and the absolute power (the Rabi frequency), or the modulation phase $\varphi(\Omega)$. Analysis of the line of the phase $\psi(\Omega)$ yields additional information, since the absolute value of φ does not influence the shape and relative variation $\Delta\psi(\Omega)$ along the line contour. The signal from the base line, which is not related to absorption, can also contribute to the error of determining the absolute values $I_{\cos_2}(\Omega, \varphi)$ and $I_{\sin_2}(\Omega, \varphi)$ of the signals and, therefore, the sign of variation in $\psi(\Omega)$ [2]. Thus, complete analysis of the line shape in the nonlinear regime requires an adequate theoretical model, knowledge of the radiation parameters and the studied spectral transitions, and obtaining experimental dependences on the radiated power, modulation frequency, and gas pressure.

Let us consider the possible influence of the group-velocity dispersion on the line shape. Radiation with the frequency ω propagates in the medium with the phase velocity $V_{\mathrm{p}} = \omega/k$, where $k = n\omega/c_0$

is the wave number, n is the refractive index of the medium, and c_0 is the speed of light. The group velocity $V_g = \partial\omega/\partial k$ is the wave-packet propagation velocity (in the case of pulsed radiation, it is the pulse-propagation velocity in the medium). It is usually smaller than the phase velocity, i.e., the light-wave front (or modulation) moves slower than the carrier-frequency wave, and the phase delay for the modulated radiation is maximum at the spectral-line center. In this case, the delay increases with narrowing line. This refers to normal dispersion. For the spectral absorption lines, dispersion at the line center is usually anomalous [36]. In the case of the Lamb dip, dispersion at the center line is usually normal. Since the modulation-phase variation along the line contour in the case of nonlinear absorption can be complex, we now estimate the maximum variation in the group velocity and modulation phase for the regions with normal dispersion.

As an example, we consider the CO-molecule line $J = 3 \leftarrow 2$ with a frequency of 345 GHz at the pressure $p = 250$ Torr ($\Delta\nu_L \approx 780$ MHz), for which not only the absorption index, but also the refractive index were measured in [36]: $\Delta\alpha \approx 7 \cdot 10^{-3}$ cm^{-1} and $\Delta k \approx 4 \cdot 10^{-3}$ cm^{-1}. Therefore, $\Delta k \approx \Delta\alpha$, which agrees with the Kramers–Kronig relation $\Delta n \sim (c_0/\omega)\,\Delta\alpha$. In this case, the radiation-phase increment (in the case considered, $2L_0 = 400$ cm) is about $\Delta\Phi \approx 1$ rad, the group velocity $V_g \sim 0.98c_0$, and the modulation-phase increment amounts to $\Delta\varphi \approx 10^{-3}$ rad for $\nu_m = 10$ kHz.

In the Doppler limit at the pressure $p = 1$ mTorr ($\Delta\nu \approx 400$ kHz), we obtain $\Delta\alpha \approx \Delta k \approx 10^{-4}$ cm^{-1} from the estimate of the refractive index using the known absorption. The radiation-phase increment is $\Delta\Phi \approx 4 \cdot 10^{-2}$ rad, the group velocity $V_g \sim 0.3c_0$, and the modulation-phase increment $\Delta\varphi \approx 3 \cdot 10^{-3}$ rad ($\nu_m = 10$ kHz).

For the Lamb dip, $\Delta k \approx \Delta\alpha = [(1+G)^{-1/2} - (1+2G)^{-1/2}]\alpha_0$ (α_0 is the absorption coefficient at the Doppler-line center). The maximum contrast is attained for $G = 1.4$ and amounts to $\Delta\alpha \approx 0.13\alpha_0$. Although the absorption variation is smaller, the linewidth of the Lamb dip (for the considered measurements, the typical half width $\gamma \approx 10$ kHz) is much smaller than the Doppler one. Therefore, the estimated group velocity $V_g \approx 0.1c_0$, the modulation phase $\Delta\varphi \approx 10^{-2}$ rad, and the radiation phase $\Delta\Phi \approx 5 \cdot 10^{-3}$ rad.

Note that the values of the modulation-phase increment starting from about $\Delta\varphi \approx 10^{-3}$ rad are well recorded. For the signal-to-noise ratios about 10^4, variation in the group velocity at the line center during reception by the modulation method can be manifested as the line-profile distortion. In addition, according to [32], in the regime of the nonlinear line saturation, a decrease in the absorption-line amplitude $\Delta\alpha = \alpha_0(1+G)^{-1/2}$ occurs in the Doppler limit for $G > 1$, whereas the dispersion-line amplitude does not change, i.e., the Kramers–Kronig relations are not fulfilled. For the Lamb dip, dispersion varies at a higher rate than absorption, i.e., $\Delta k(G) \approx 0.45[G/(1+G)]\alpha_0$ [34]. Therefore, a still greater group-velocity slowing down and an increase in the delay of the modulation phase at the line center are possible for the line-saturation regime.

Let us note the nonmonotonic dependence of the Lamb-dip amplitude and phase $\Delta\psi(\Omega)$ on the gas pressure. If pressure decreases to about 1 mTorr, the signal related to the Lamb dip increases at the second harmonic of the modulation frequency (e.g., the CO-molecule line $J = 1 \leftarrow 2$), which is due to a decrease in the half width Γ and an increase in the saturation degree ($G = (g/\Gamma)^2$). With the further pressure decrease (in the case considered, this coincides with the transition to the region of the transit effects), the line width γ is actually remained unchanged, while the line-related signal started to decrease. Therefore, as pressure decreases to 1.0–1.5 mTorr, the signal value $\Delta\psi(\Omega)$ also increases, but at a higher rate, and then drops. At a pressure of about 1.3 mTorr, the sign of the Lamb-dip phase is reversed. Although the relative increase $\Delta\psi(\Omega)$ is related to variation in the ratio ν_m/Γ, its dependence on the saturation degree is possible, as is shown in [34].

Let us consider the influence of coherent effects on the line shape. Figure 4 shows the line record for the modulation frequencies exceeding the resonance width ($\nu_m/\gamma > 1$) for two values of the radiated power $P_1 > P_0$. An increase in the radiation intensity leads to an increase in the beat intensity at the Doppler-contour center, which is related to the rise of both the Rabi frequency and the probability of inverse stimulated transition of particles to the lower level. Apart from the beat-intensity increase, the line

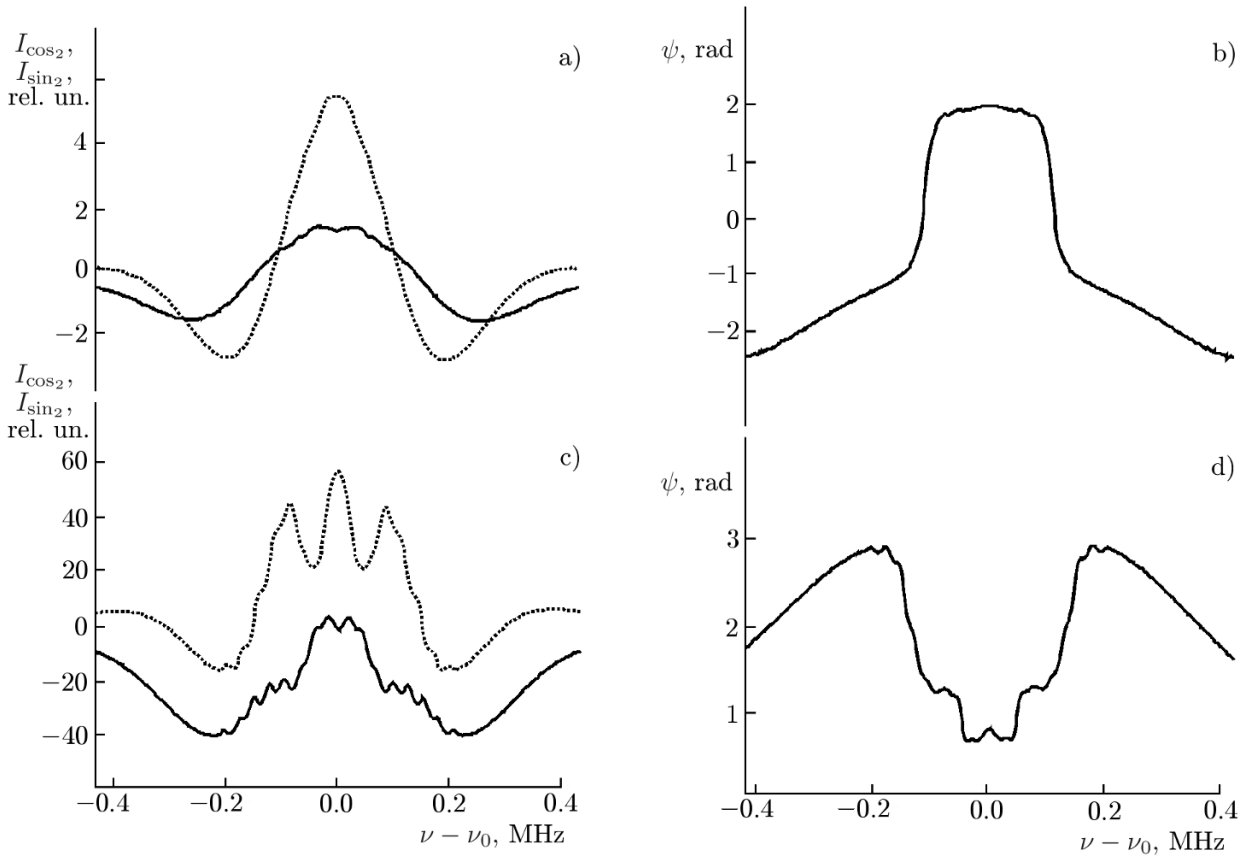

Fig. 4. The dependences of the amplitude shape (*a* and *c*; the solid lines correspond to the channel $I_{\cos_2}$ and the dashed lines, to $I_{\sin_2}$) and the phase (*b* and *d*) of the signal related to the OCS-molecule line (145 GHz and $J = 12 \leftarrow 11$) in the case $\nu_{\rm m}/\gamma > 1$ for the modulation frequency $\nu_{\rm m} = 50$ kHz and two values of the radiated power $P = P_0$ (*a* and *b*) and $P = P_1$ (*c* and *d*) if $P_1 > P_0$, $\Delta = 120$ kHz, $p \approx 0.5$ mTorr.

of the phases $\psi(\Omega)$ also demonstrates a significant decrease in the phase at the line center with increasing power (see Fig. 4*b*), which is similar to that observed in Fig. 3.

To conclude, it should be noted that for the sub-Doppler saturation spectroscopy in the case of a high modulation frequency ($\nu_{\rm m}/\gamma \geq 1$), the absorption line becomes more complex [37, 38] and the resonances are observed at the frequencies $\nu_0 \pm m\nu_{\rm m}/2$. This can also explain the beats observed in Fig. 4.

Because of the ambiguity of interpretation of many experimental dependences and lack of a comprehensive theoretical model, in this work we have only delineated the scope of possible physical effects which can lead to the above-discussed observation results. The study of the nonlinear saturation resonance for an arbitrary modulation frequency with respect to the linewidth should be continued.

4. CONCLUSIONS

The influence of the saturation effects of the spectral lines on the value and shape of the recorded frequency-modulated signals in the quadrature channels during synchronous detection has been experimentally demonstrated. In the nonlinear regime, a variation in the relationship between dispersion and absorption, which are interrelated by the Kramers–Kronig formulas in the linear case, has been observed. The necessity of allowing for the influence of the group-velocity dispersion and coherent effects on the shape of the recorded spectral lines in the saturation regime has been shown. As far as we know, consideration of the possible influence of the group-velocity decrease on the line shape during the modulation reception method and analysis of the phase difference for the signals in the quadrature channels have been performed for the first time in this work.

We sincerely thank A. P. Shkaev and A. F. Andriyanov for technical support of the measurements.

This work was partially supported by the Russian Foundation for Basic Research (project Nos. 16-02-00761_a and 15-02-07887_a)), the Program of Fundamental Research "New sources of millimeter and terahertz radiation and their promising applications" of the Branch of Physical Sciences of the Russian Academy of Sciences, and State Assignment No. 0035–2014–0009.

REFERENCES

1. G. Yu. Golubiatnikov, S. P. Belov, I. I. Leonov, et al., *Radiophys. Quantum Electron.*, **56**, Nos. 8–9, 599 (2013).
2. G. Yu. Golubiatnikov, S. P. Belov, and A. V. Lapinov, *Radiophys. Quantum Electron.*, **58**, No. 8, 622 (2015).
3. A. V. Lapinov, S. A. Levshakov, M. G. Kozlov, et al., *RFBR Bull.*, No. 1(73), 111 (2012).
4. V. S. Letokhov and V. P. Chebotaev, *Sov. Phys. Uspekhi*, **17**, No. 4, 467 (1975).
5. V. P. Kochanov, S. P. Belov, and G. Yu. Golubiatnikov, *J. Quant. Spectrosc. Rad. Transfer*, **149**, 146 (2014).
6. R. Karplus, *Phys. Rev.*, **73**, No. 9, 1027 (1948).
7. S. N. Bagaev, E. V. Baklanov, and V. P. Chebotaev, *JETP Lett.*, **16**, No. 1, 9 (1972).
8. T. O. Meyer and C. K. Rhodes, *Phys. Rev. A*, **12**, No. 5, 1993 (1975).
9. V. P. Kochanov, S. G. Rautian, and A. M. Shalagin, *Sov. Phys. JETP*, **45**, No. 4, 714 (1977).
10. V. P. Kochanov, *JETP*, **118**, No. 3, 335 (2014).
11. S. N. Bagaev and V. P. Chebotaev, *Sov. Phys. Uspekhi*, **29**, No. 1, 82 (1986).
12. S. N. Bagayev, V. P. Chebotayev, and E. A. Titov, *Laser Phys.*, **4**, No. 2, 224 (1994).
13. C. J. Borde, J. L. Hall, C. V. Kunasz, and D. G. Hummer, *Phys. Rev. A*, **14**, No. 1, 236 (1976).
14. S. N. Bagayev, V. P. Chebotayev, A. K. Dmitriyev, et al., *Appl. Phys. B*, **52**, 63 (1991).
15. Ch. Chardonnet, F. Guernet, G. Charton, Ch. Bord, *J. Appl. Phys. B*, **59**, No. 3, 333 (1994).
16. S. L. McCall and E. L. Hahn, *Phys. Rev. Lett.*, **18**, No. 21, 908 (1967).
17. P. G. Kryukov and V. S. Letokhov, *Sov. Phys. Uspekhi*, **12**, No. 5, 64 (1970).
18. J. M. Supplee, E. A. Whittaker, and W. Lenth, *Appl. Opt.*, **33**, No. 27, 6294 (1994).
19. G. C. Bjorklund, M. D. Levenson, W. Lenth, and C. Ortiz, *Appl. Phys. B*, **32**, No. 3, 145 (1983).
20. S. W. North, X. S. Zheng, R. Fei, and G. E. Hall, *J. Chem. Phys.*, **104**, No. 6, 2129 (1996).
21. L.-S. Ma, J. Ye, P. Dube, and J. L. Hall, *J. Opt. Soc. Am. B*, **16**, No. 12, 2255 (1999).
22. A. Foltynowicz, F. M. Schmidt, W. Ma, and O. Axner, *Appl. Phys. B*, **92**, No. 3, 313 (2008).
23. P. Kluczynski and O. Axner, *Appl. Opt.*, **38**, No. 27, 5803 (1999).
24. P. Kluczynski, J. Gustafsson, A. M. Lindberg, and O. Axner, *Spectrochim Acta B*, **56**, 1277 (2001).
25. J. P. M. De Vreede, S. C. Mehrotra, A. Tal, and H. A. Dijkerman, *Appl. Spectrosc.*, **36**, No. 3, 227 (1982).
26. H. Wahlquist, *J. Chem. Phys.*, **35**, No. 5, 1708 (1961).
27. R. Arndt, *J. Appl. Phys.*, **36**, No. 8, 2522 (1965).
28. J. Reid and D. Labrie, *Appl. Phys. B*, **26**, No. 3, 203 (1981).
29. P. Kluczynski, A. M. Lindberg, and O. Axner, *J. Quant. Spectrosc. Rad. Transfer*, **83**, Nos. 3–4, 345 (2004).

30. L. Dore, *J. Mol. Spectrosc.*, **221**, 93 (2003).
31. E. De Tommasi, A. Castrillo, G. Casa, and L. Gianfrani, *J. Quant. Spectrosc. Rad. Transfer*, **109**, No. 2, 168 (2008).
32. W. Ma, A. Foltynowicz, and O. Axner, *J. Opt. Soc. Am. B*, **25**, No. 7, 1144 (2008).
33. A. Foltynowicz, W. Ma, F. M. Schmidt, and O. Axner, *J. Opt. Soc. Am. B*, **25**, No. 7, 1156 (2008).
34. O. Axner, W. Ma, and A. Foltynowicz, *J. Opt. Soc. Am. B*, **25**, No. 7, 1166 (2008).
35. A. V. Matsko, O. Kocharovskaya, Y. Rostovstev, et al., *Adv. Atom. Mol. Opt. Phys.*, **46**, 191 (2001).
36. M. N. Afsar, H. Chi, and H. Sobhie, in: *Proc. SPIE., San Diego, USA, January 10, 1994*, Vol. 2211, p. 768.
37. G. C. Bjorklund and M. D. Levenson, *Phys. Rev. A*, **24**, No. 1, 166 (1981).
38. A. Schenzle, R. G. DeVoe, and R. G. Brewer, *Phys. Rev. A*, **25**, No. 5, 2606 (1982).